Supplementary materials for

Ubiquitin-mediated degradation of ANP32A by Realgar licenses ferritinophagic ferroptosis in TNBC stem cells through an ATG5-dependent epigenetic program

Manman Wang[a,1,*], Sufeng Zhang[a,1], Mingjie Zhao[a], Jiejie Sun[b], Meng Wang[a], Hui Cheng[a], Zhiye Zhang[c,*], An Zhou[a,d,*]

[a] Key Laboratory of Xin'an Medicine, Ministry of Education, Anhui University of Chinese Medicine; Hefei 230038, China

[b] BoZhou Vocational and Technical College, Bozhou, 236800, China

[c] Fuyang Hospital of Anhui Medical University, Fuyang, 236000, China

[d] School of Pharmacy, Anhui University of Chinese Medicine, Hefei, 230038, China.

[*] Corresponding authors.

[1] These authors contributed equally.

E-mail addresses: mm-wang@ahtcm.edu.cn (Manman Wang), anzhou@ahtcm.edu.cn. (An Zhou) , 13505588957@163.com (Zhiye Zhang)

Supplementary table1. The primers used for qRT-PCR analysis and the siRNA sequences specifically targeting ATG5, STUB1, and NCOA4 are listed below.

Name	***sequences(5'-3')***
ANP32A Forward	*CAGCAGCAGCTCCAGAAG*
ANP32A Reverse	*GGATGGCGTTCTCCAGTA*
ATG5 Forward	*TGTCTTCGAAGATGACAGACTCG*
ATG5 Reverse	*ACCAAACAACGTGAGCTGTGTAG*
ALDH1A1 Forward	*CCAGGACCTGGCAACTTGTA*
ALDH1A1 Reverse	*CCAAAGTTGCAGCCATACCA*
CD44 Forward	*GCATTGCAGTCAACAGTCGAAGA*
CD44 Reverse	*CCTTGTTCACCAAATGCACCA*
NANOG Forward	*CGAGATAAACATGGCAATCAAAAT*
NANOG Reverse	*AATTCAGCAAGAAGCCTCTCCTT*
OCT4 Forward	*GGGATATACACAGGCCGAT*
OCT4 Reverse	*GATACTGGTTCGCTTTCTCT*
SOX2 Forward	*CGAGTAGGACATGCTGTAGGT*
SOX2 Reverse	*TGGACAGTTACGCGCACAT*
GAPDH Forward	*ATCAAGTGGGGCGATGCTG*
GAPDH Reverse	*ACCCATGACGAACATGGGG*
ATG5 siRNA	*AUCUUCUUGUCUCAUAACCTT*
STUB1 siRNA	*AUACAUGGCAGAUAUGGAUTT*
NCOA4 siRNA	*GACCUUAUUUAUCAGCUUATT*

Supplementary table2. The top DEPs included in the heatmap presented in Figure 3D

Description	Gene	Realgar vs.ctr Pvalue	Realgar vs.ctr log2FC	Realgar vs.ctr UP/DOWN
Alternative protein MKKS	MKKS	0.042381069	-5.673076807	down
COX assembly mitochondrial protein homolog	CMC1	6.25E-05	-4.17784256	down
Cystatin-SN	CST1	0.025768176	-4.099017841	down
Acidic leucine-rich nuclear phosphoprotein 32 family member A	**ANP32A**	**0.02418097**	**-3.88923238**	**down**
40S ribosomal protein S27	RPS27L	0.00746013	-3.651988723	down
Medium-chain acyl-CoA ligase ACSF2, mitochondrial	ACSF2	0.009780889	-3.441514117	down
gamma-glutamylcyclotransferase	GGCT	0.031301013	-3.41097198	down
CHTM1	CHTM1	0.017890407	-3.372662031	down
Leucine-rich repeat-containing protein 39	LRRC39	0.010307171	-2.809421471	down
MHC class I antigen	HLA-C	0.006125465	-2.781425958	down
Interferon regulatory factor 2-binding protein 2	IRF2BP2	0.034618408	-2.749857361	down
Endothelial differentiation-related factor 1	EDF1	0.006228101	-2.716656719	down
39S ribosomal protein L28, mitochondrial (Fragment)	MRPL28	0.006324954	-2.650943098	down
Chondroitin sulfate proteoglycan 4	CSPG4	0.000129342	-2.614719898	down
Carnitine O-acetyltransferase	CRAT	0.024052835	-2.527840698	down
Epididymis secretory protein Li 114	HEL-S-114	0.003410999	-2.487086794	down
Transcription factor Sp3 (Fragment)	SP3	0.027894221	-2.463382087	down
CCR4-NOT transcription complex subunit 2	CNOT2	0.017887182	-2.442858187	down
t-plasminogen activator	PLAT	0.013549728	-2.435068599	down

Supplementary figures

Figure S1. The TEM images revealed that the particle size of Realgar (related to Fig. 1).

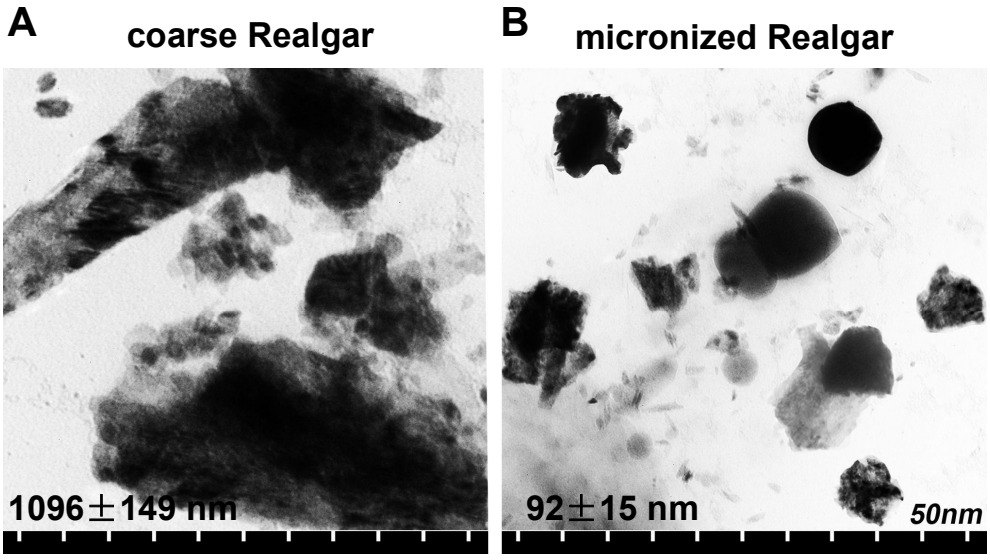

(A, B) TEM images of coarse Realgar and micronized Realgar prepared from the optimum condition. (A) Coarse realgar; (B) micronized Realgar. Abbreviations: TEM, transmission electron microscopy.

Figure S2. Realgar impairs migration and CSC maintenance in TNBC (related to Fig. 1).

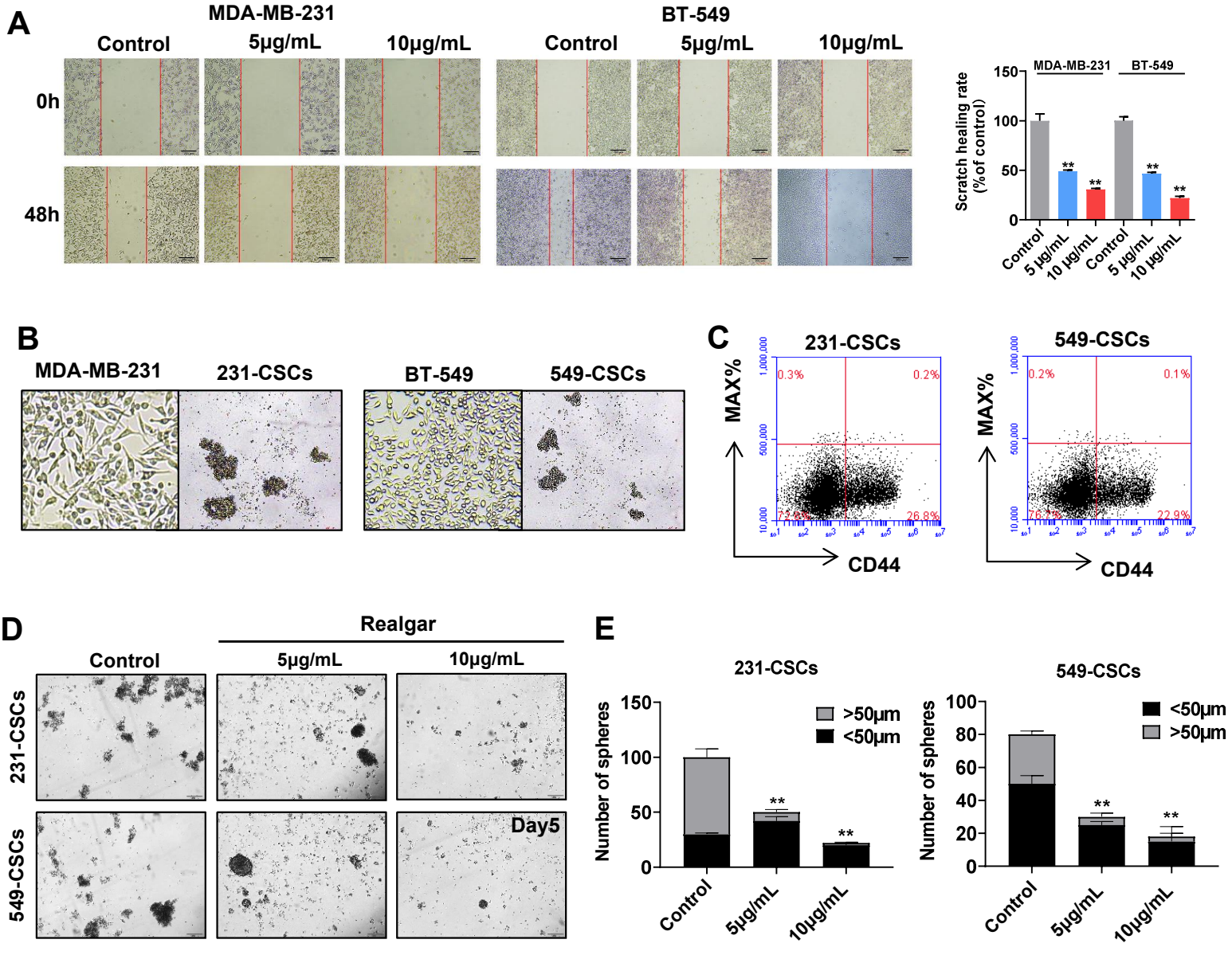

(A) Wound healing assay were conducted to determine the cell migration in MDA-MB-231 and BT-549 cell lines following treatment with Realgar at concentrations of 0, 5, and 10 μg/mL for 48 hours (scale bar = 200 μm).

(B) Human TNBC stem cell lines (231-CSCs and 549-CSCs) were enriched from MDA-MB-231 and BT-549 cells through multiple rounds of sphere-forming culture. Images of 231-CSC and 549-CSC spheroids were captured using a light microscope (Scale bar=200 μm).

(C) The proportion of $CD44^+$ cells in the enriched 231-CSCs and 549-CSCs was subsequently analyzed using flow cytometry.

(D, E) A sphere-forming assay was performed on 231-CSCs and 549-CSCs that were treated with or without Realgar at the designated concentration (Scale bar = 200 μm), and the total number of spheroids was recorded. Data are presented as mean ± SEM; *$p < 0.05$, **$p < 0.01$ versus control.

Figure S3. Realgar significantly reduced the CD44^{+}CD24^{-} population in 549-CSCs and 231-CSCs (related to Fig. 1).

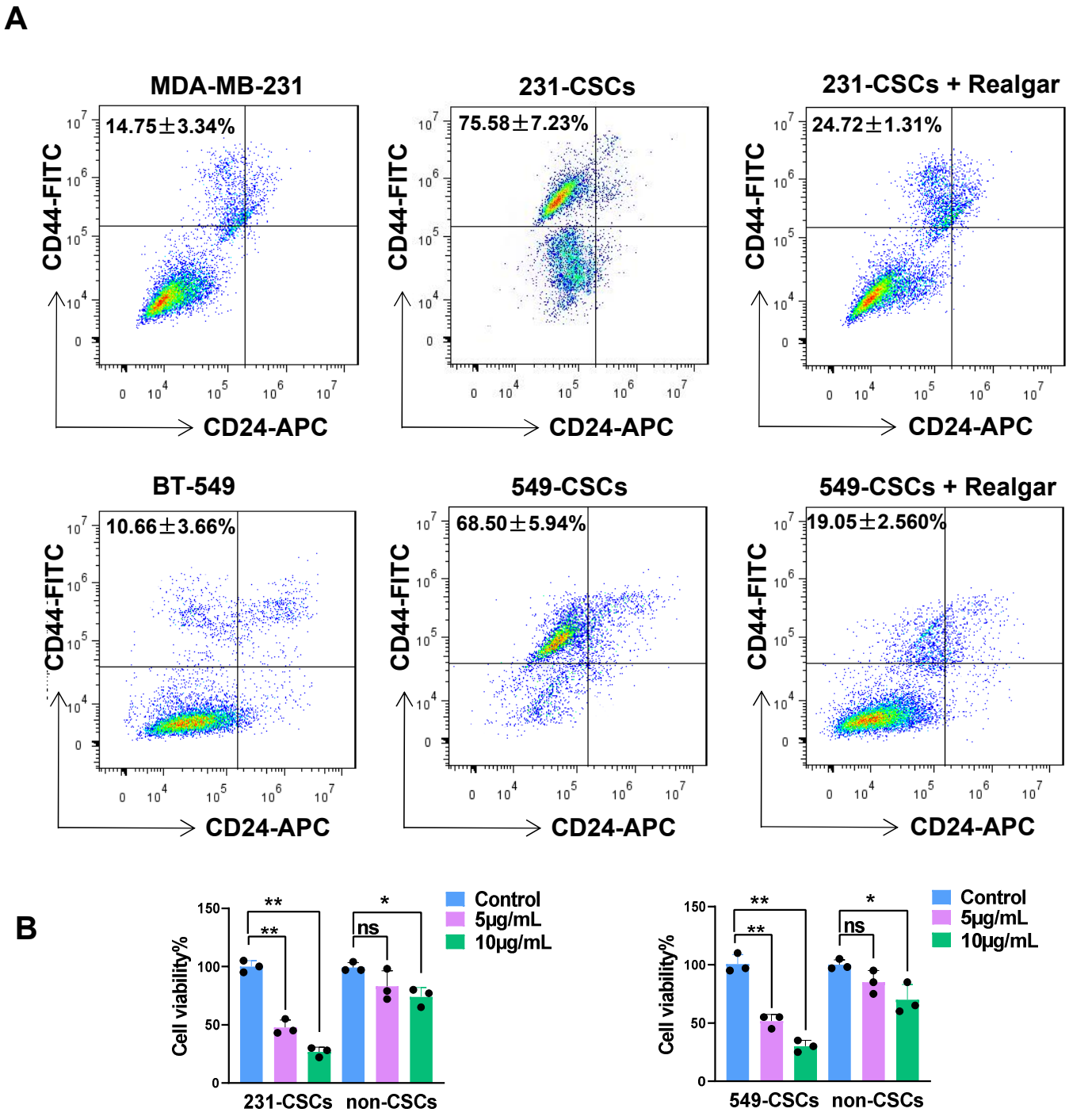

(A) The proportion of CD44^{+}CD24^{-} cells in MDA-MB-231, BT-549, as well as in the enriched 231-CSCs and 549-CSCs, with or without treatment of Realgar (10μg/mL), was analyzed using flow cytometry. Data are presented as mean ± SEM

(B) The cell viability of enriched 231-CSCs and 549-CSCs (CD44^{+}CD24^{-}), as well as non-CSCs (CD44^{-}CD24^{+}), was determined using the CCK-8 assay after a 48 hour treatment with Realgar. Data are presented as mean ± SEM; *$p < 0.05$, **$p < 0.01$ versus control.

Figure S4. The serum ALT, AST, BUN and creatinine were measured to assess hepatic and renal function in MDA-MB-231 xenograft model after Realgar treatment (related to Fig. 2).

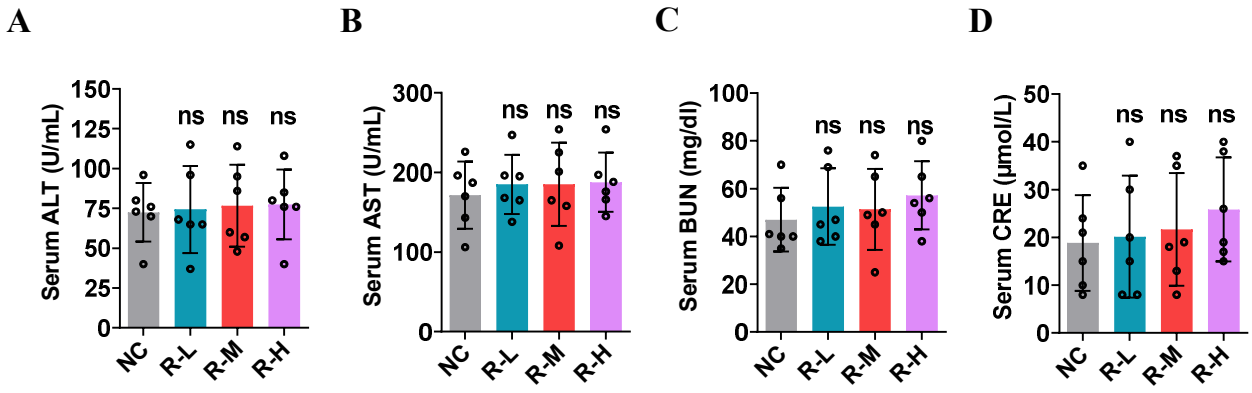

(A-D) Serum levels of alanine aminotransferase (ALT), aspartate aminotransferase (AST), blood urea nitrogen (BUN), and creatinine (CRE) were measured in the xenograft model (n=6 mice per group). Data are presented as the mean±SEM; non-significant (ns) when $p > 0.05$, *$p < 0.05$, and **$p < 0.01$ compared to the control group.

Figure S5. E3 ligase recognition motif for the substrate ANP32A (K20 and K99) in Homo sapiens (related to Fig. 4)

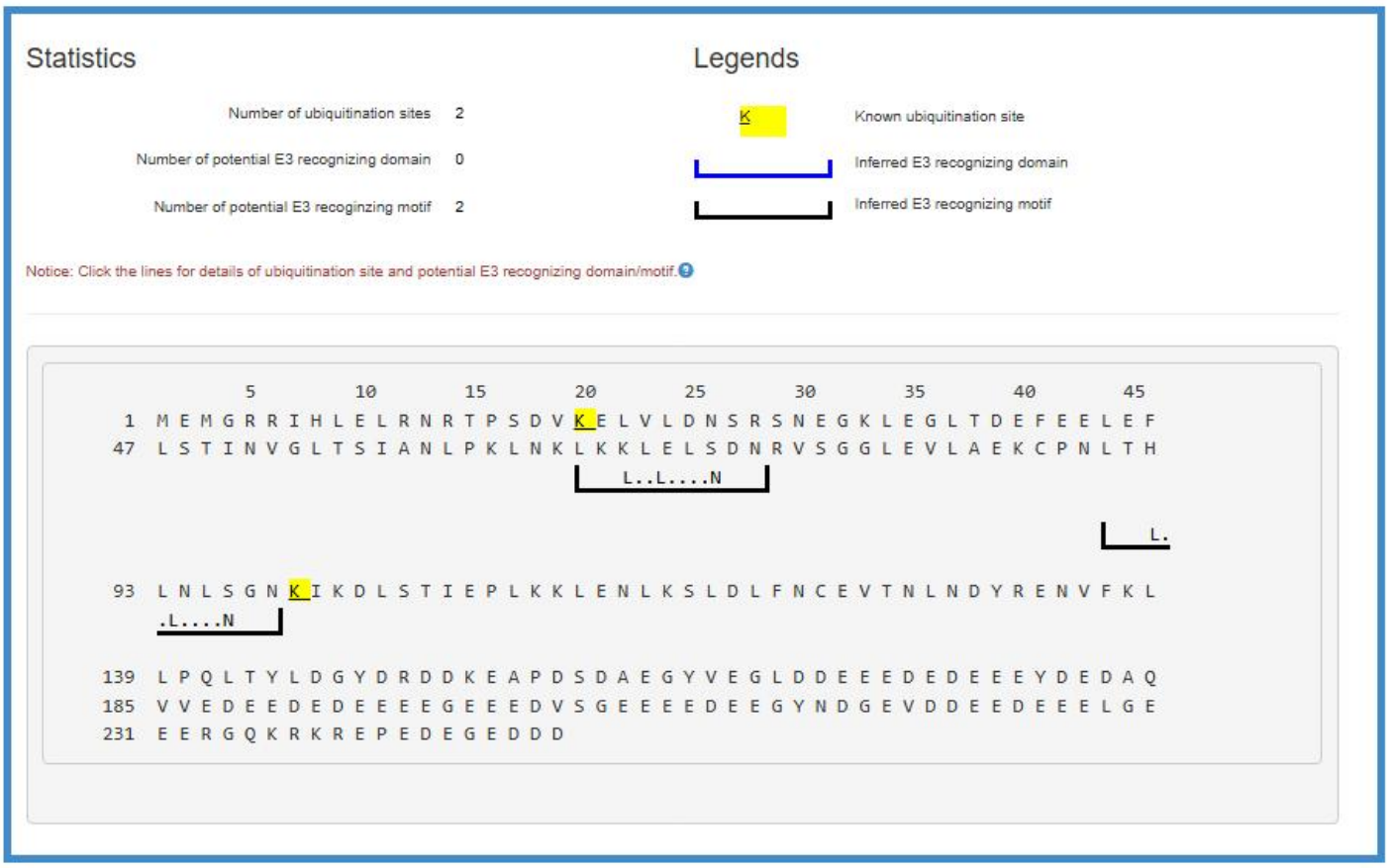

(A) Utilize the Ubibrowser tool to predict the recognition motif for the substrate ANP32A (K20 and K99), which is mediated by E3 ligase in Homo sapiens (http://ubibrowser.bio-it.cn/ubibrowser_v3/home/index).

Figure S6. Identification of the E3 ligase responsible for Realgar-induced ANP32A ubiquitination (related to Fig. 4)

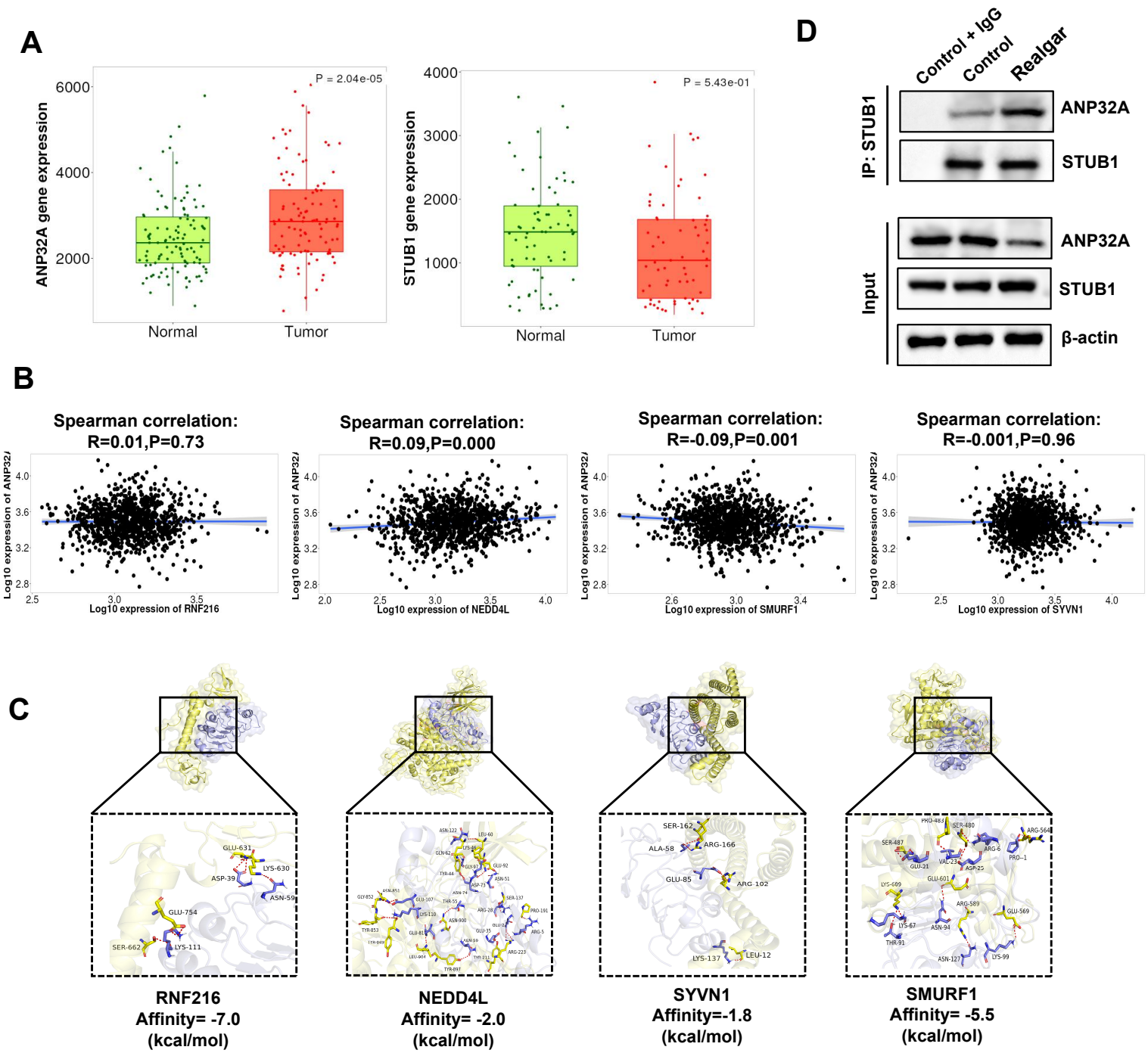

(A, B) Gene expression levels of ANP32A and STUB1, as well as Spearman correlation analysis between ANP32A and selected E3 ubiquitin ligases (RNF216, NEDD4L, SYVN1, and SMURF1), based on TNMplot v2 microarray data.

(C) A molecular docking analysis using GRAMM demonstrated the interactions between ANP32A and these proteins. The combined free energy was calculated by means of PDBePISA and visualized with PyMOL 3.1. ANP32A is represented in yellow, and the E3 is portrayed in blue.

(D) Co-immunoprecipitation (Co-IP) with an anti-STUB1 antibody was utilized to examine the effect of Realgar treatment on the direct interaction between endogenous ANP32A and the E3 ligase STUB1. IgG was used as a negative control for the pulldown. Whole-cell lysates were used as input controls.

Figure S7. ANP32A expression in TNBC patients based on TCGA database analysis (related to Fig. 5).

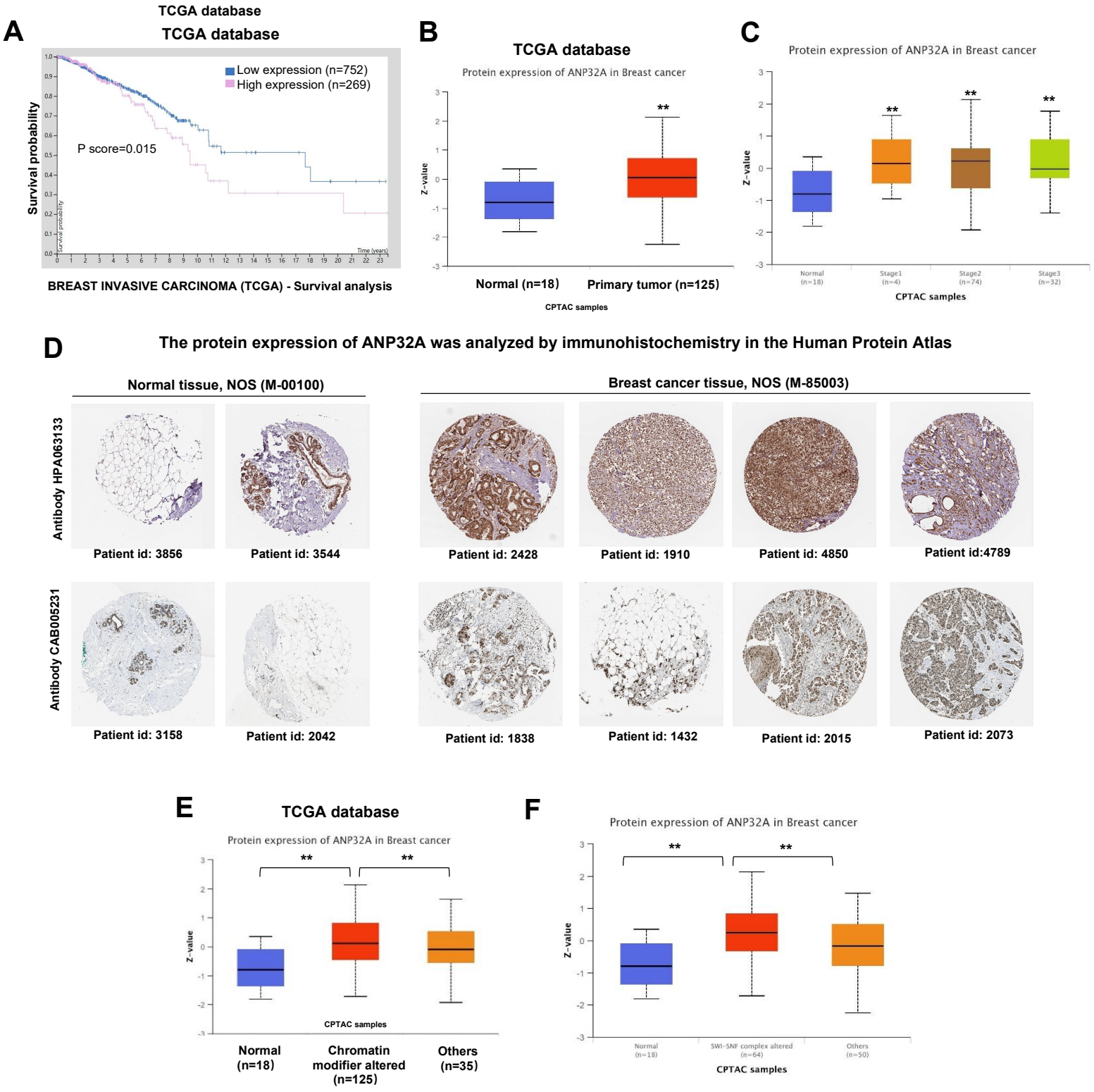

(A, B) The TCGA database was utilized to assess ANP32A mRNA expression across BC and perform survival analysis for patients with varying ANP32A expression levels, based on TCGA database analysis.

(C, D) Protein expression of ANP32A at different stages of breast cancer were analyzed in the Human Protein Atlas.

(E, F) Abnormally elevated ANP32A expression was identified in BC patients exhibiting chromatin modification alterations and SWI/SNF complex alterations.

Figure S8. ANP32A maintains CSC properties and mediates Realgar's antitumor efficacy (related to Fig. 6).

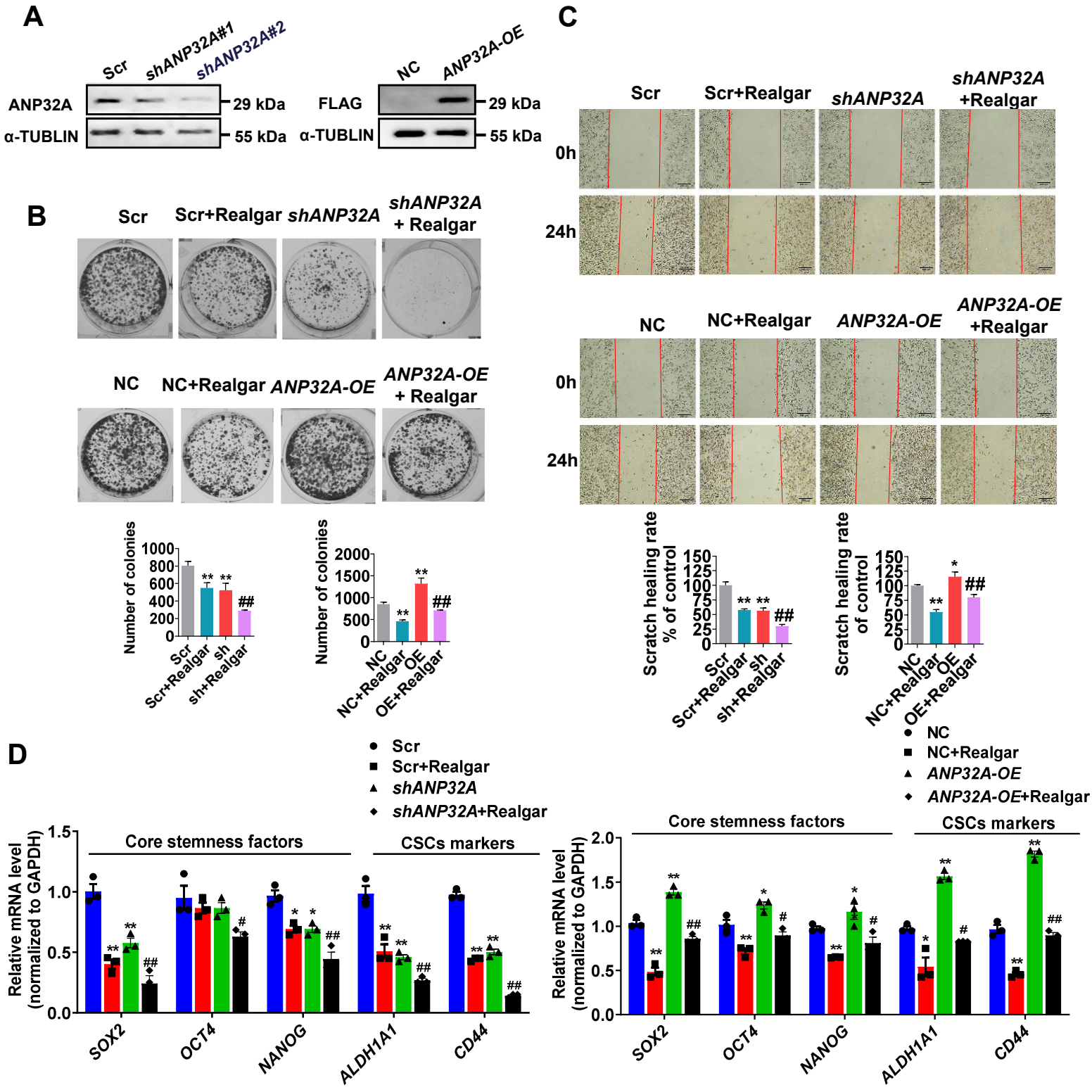

(A) Knockdown (Scr, shANP32A) or overexpression of ANP32A (NC, ANP32A-OE) was conducted in MDA-MB-231 cells, and the modulation efficiency of ANP32A was confirmed by Western blot analysis.

(B, C) The colony formation and wound healing assay were performed at 0 and 48 hours to evaluate the effect of ANP32A on Realgar-mediated inhibition of TNBC cell migration (scale bar = 200 μm).

(D) The expression levels of core stemness-related genes (SOX2, OCT4, NANOG) and CSC-associated markers (CD44, ALDH1A1) were analyzed using qRT-PCR. Data are presented as mean ± SEM; *p < 0.05, **p < 0.01 versus Scr or NC groups; #p < 0.05, ##p < 0.01 versus Scr+Realgar or NC+Realgar groups.

Figure S9. Tumor progression was evaluated through histopathological assessment of tumor tissues (related to Fig. 6).

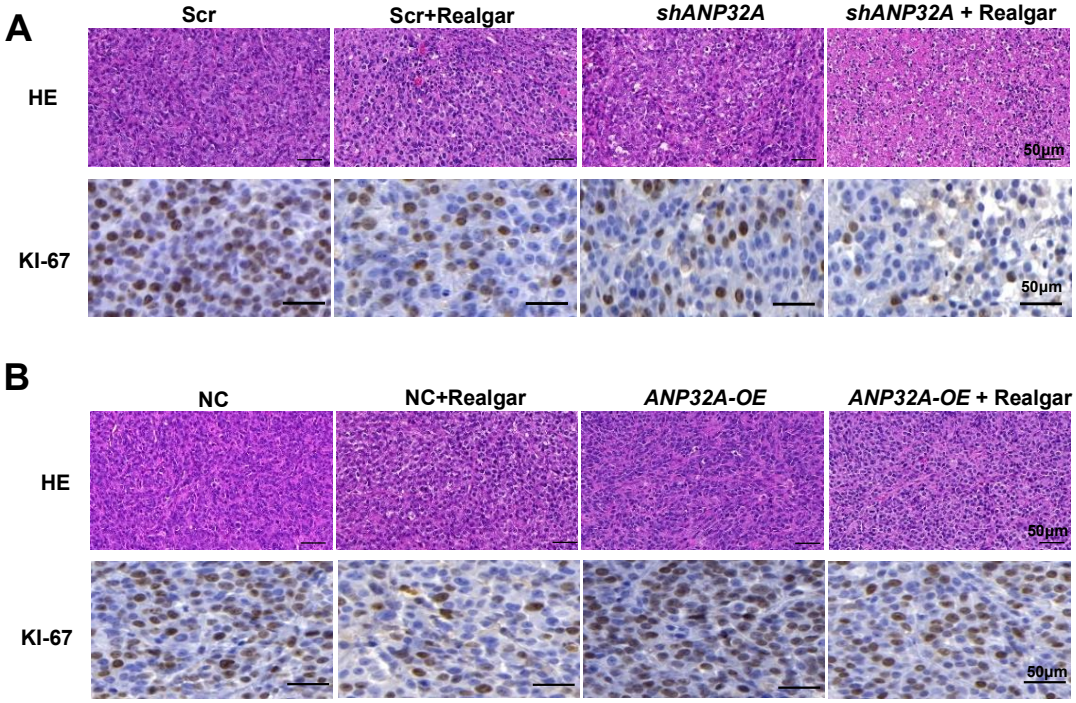

(A,B) Histopathological evaluation of tumor tissues was performed using HE staining and IHC staining for KI-67 (scale bar = 50 μm).

Figure S10. ANP32A directly bound to the promoter region of the ATG5 gene (related to Fig. 7G).

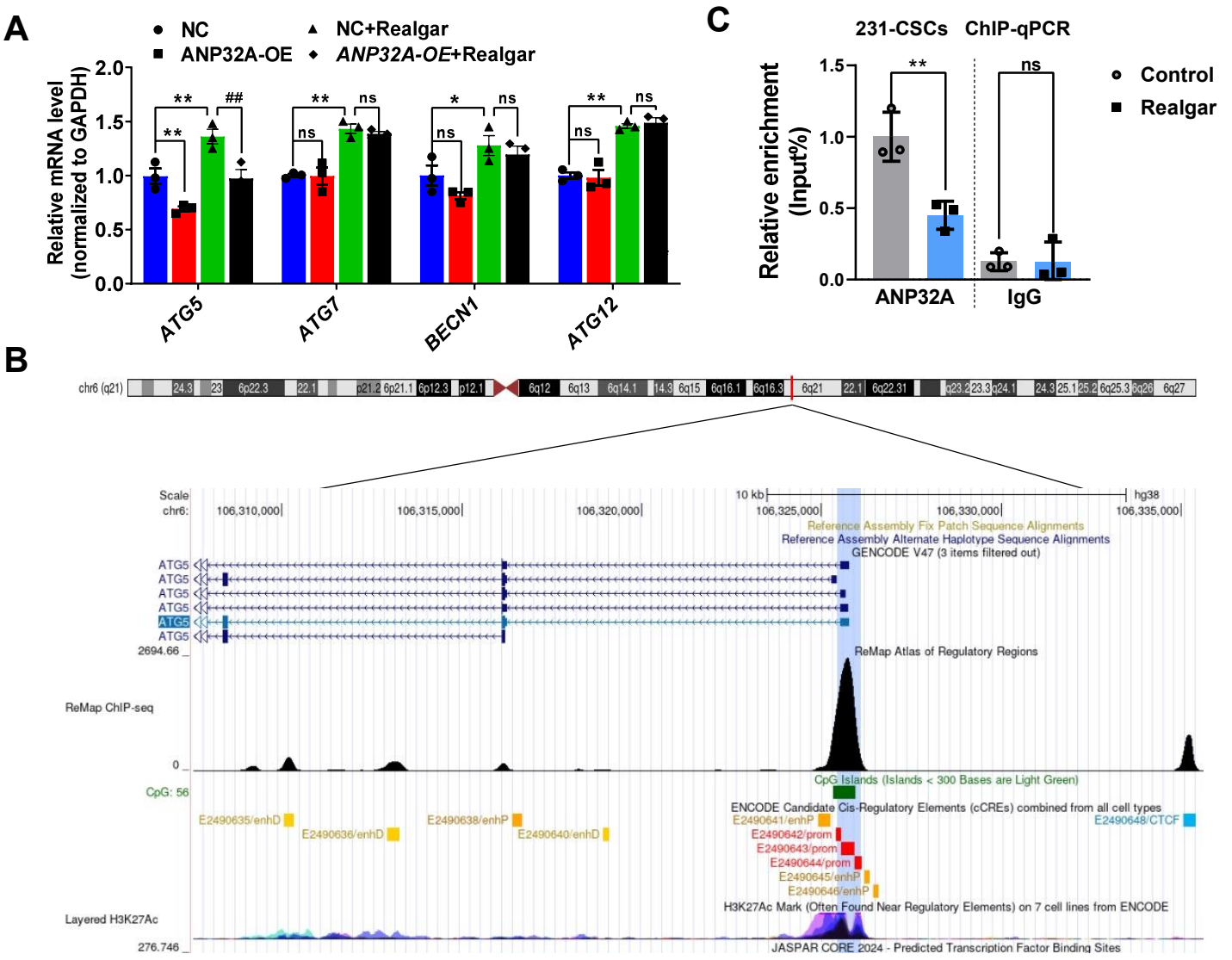

>NC_000006.12:106325392-106326104 Homo sapiens chromosome 6, GRCh38.p14 Primary Assembly

ORIGIN

1 tgtgtgatgc caggaagaaa gggatgttgc gatcaagctc tagggaggca gtgtttcagt
61 attttaaaaa ctgtttttgt ggaactgtta agttaacctc cccaagcccc aataactacg
121 ctttgacgca agattctcag aagagggtag aagctatgaa cttggagagg tttggtcgcg
181 agttcaagcg tactgccccg ttggcgcatg ctcaagagcg actcgggcct ccttgctggg
241 ttaggcagaa cacggagggc ggagttcgga ccacgtgggg tctcgtgacg tcatctccgg
301 gcgccgaggg tgactggact tgtggtgcgc tgccagggct ccgcagcgtt gccggttgta
361 ttcgctggat accagagggc ggaagtgcag cagggttcag ctccgacctc cgcgccggtg
421 ctttttgcgg ctgcgcgggc ttcctggagt cctgctaccg cgtccccgca ggacagtgtg
481 tcaggcgggc agcttgcccc gccgccccac cggagcgcgg aatctgggcg tccccaccag
541 tgcggggagc cggaaggagg agccatagct tggagtaggg tacgtgtgtg tgtccacctt
601 gtgtgaggaa attcctagag gaggagggct ggggaggggc caggtaggtg tggtaggaag
661 gaggggtgag tagttgcctg gaggagcgcc cgcccggccg cgatggcggg tga

(A) The mRNA expression levels of autophagy-related genes were analyzed by qRT-PCR in 231-CSCs to determine whether ATG5 serves as the dominant downstream effector of ANP32A. Data are presented as mean ± SEM; *p < 0.05, **p < 0.01 vs. NC; #p < 0.05, ##p < 0.01 vs. NC+Realgar.
(B) JASPAR prediction of H3K27Ac-marked regions within the human ATG5 promoter was conducted using data from the UCSC database, and the corresponding sequence information is presented.
(C) ChIP-qPCR assays using ANP32A or IgG antibodies were performed in control and Realgar-treated 231-CSCs to demonstrate the physical presence of ANP32A at the ATG5 promoter and whether Realgar treatment reduces its occupancy. Data are presented as mean ± SEM; *p < 0.05, **p < 0.01 versus the Control group.

Figure S11. Realgar-induced autophagy promotes ferritin degradation (related to Fig. 9).

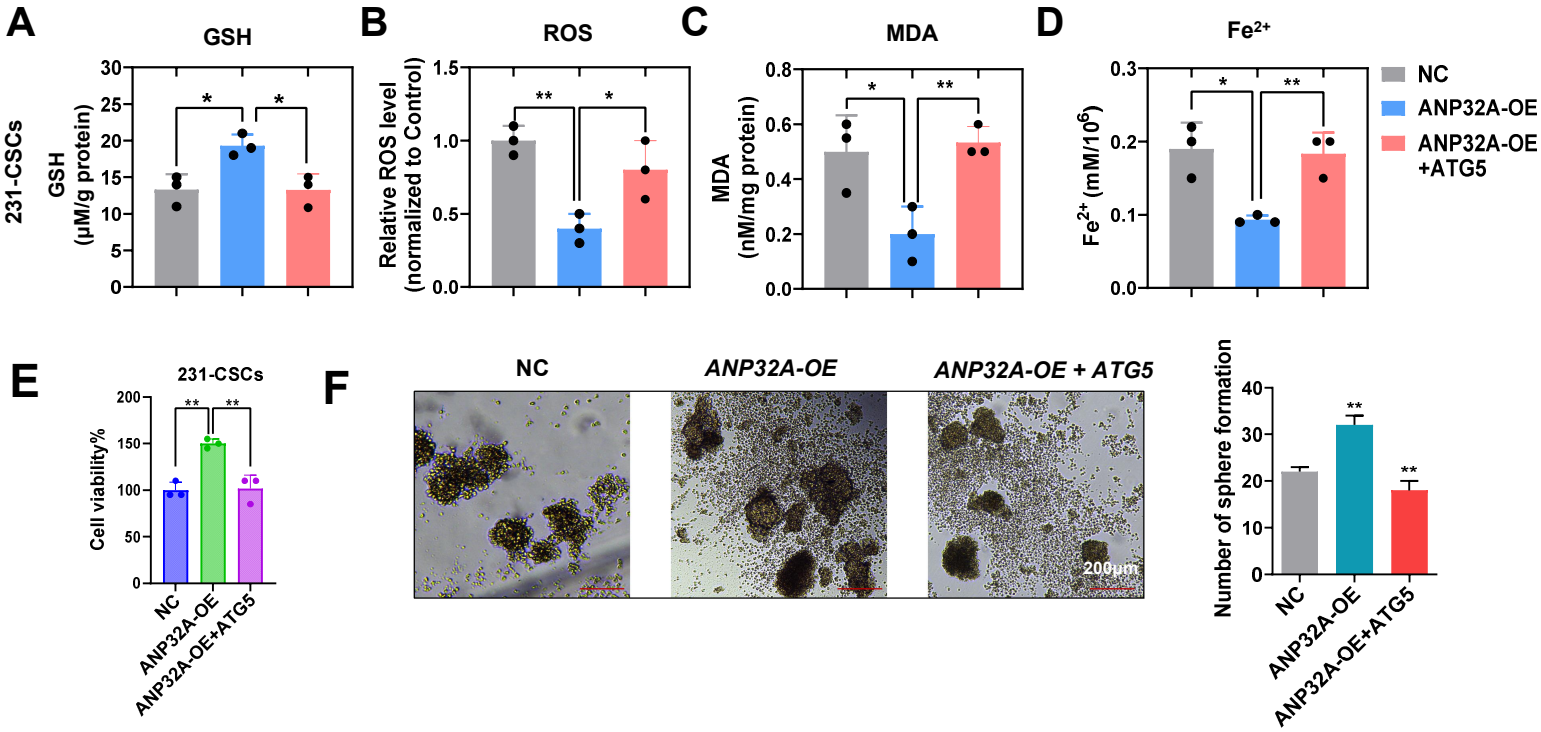

（**A**）The influence of ANP32A overexpression (ANP32A-OE) on ferroptosis and the recovery effect mediated by transient ATG5 overexpression are displayed. Data are presented as mean ± SEM; **p < 0.01, *p < 0.05 vs. ANP32A-OE.

Figure S12. siNCOA4 significantly attenuates Realgar-induced ferritinophagic ferroptosis (related to Fig. 9).

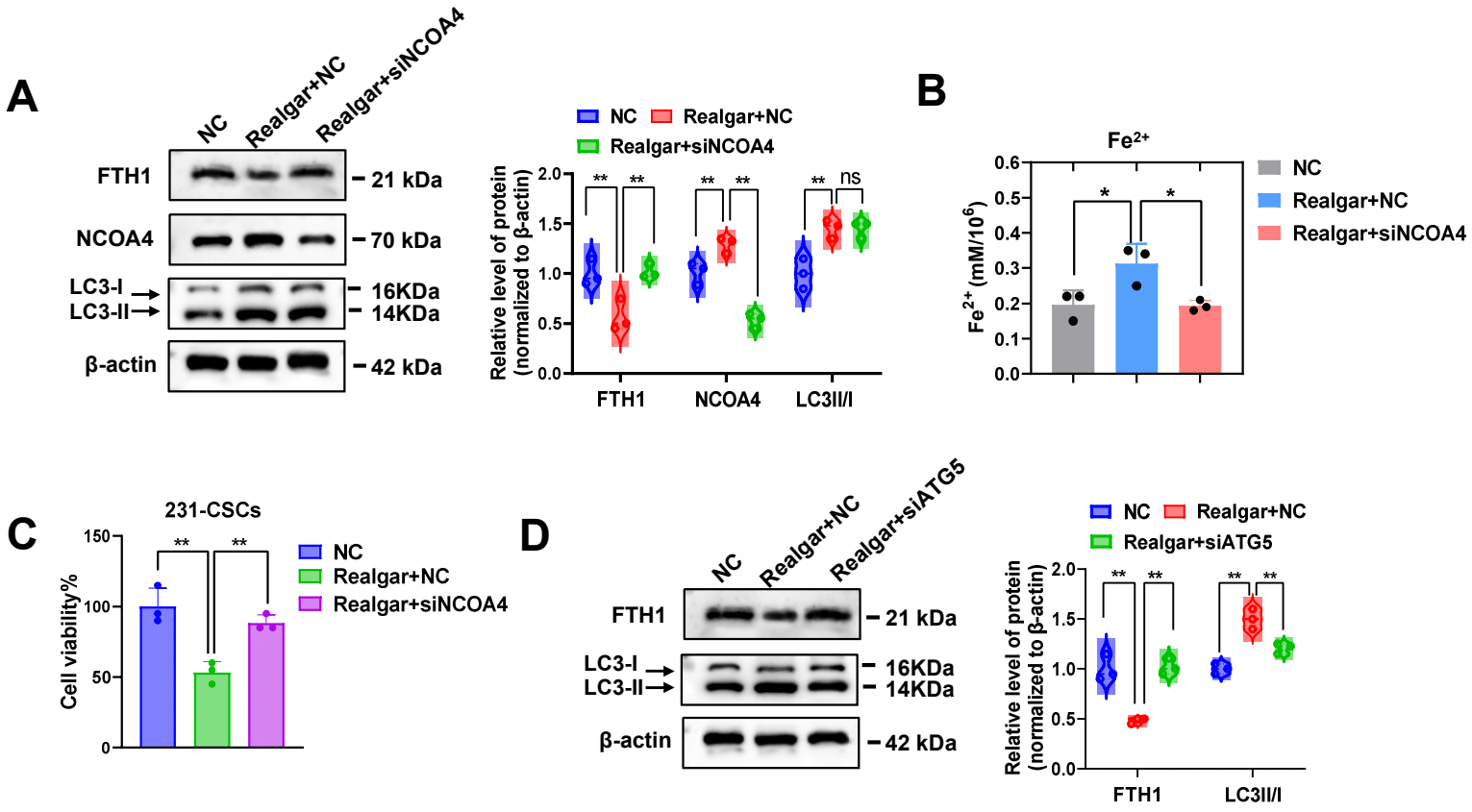

(A) Western blot analysis was carried out to detect the levels of NCOA4, LC3-I/II, and FTH1 proteins in 231-CSCs following Realgar treatment, either in the presence or absence of siNCOA4. **(B,C)** The free iron content was measured using the Fe^{2+} Assay Kit. The cell viability was assessed using the CCK-8 assay.

(D) Western blot analysis was conducted to detect the levels of LC3 - I/II and FTH1 proteins in 231 - CSCs after Realgar treatment, either with or without siATG5. Data are presented as mean±SEM; $^{**}p < 0.01$, $^{*}p < 0.05$ compared to the Realgar group.